

## Two-Photon and Time-Resolved Fluorescence Conformational Studies of Aggregation in Amyloid Peptides

Ying Wang, Travis B. Clark, and Theodore Goodson III\*

Department of Chemistry, University of Michigan, Ann Arbor, Michigan 48109

Received: February 18, 2010

The conformational changes associated with the aggregation of proteins are critical to the understanding of fundamental molecular events involved in early processes of neurodegenerative diseases. A detailed investigation of these processes requires the development of new approaches that allow for sensitive measurements of protein interactions. In this paper, we applied two-photon spectroscopy coupled with time-resolved fluorescence measurements to analyze amyloid peptide interactions through aggregation-dependent concentration effects. Labeled amyloid- $\beta$  peptide (TAMRA-A $\beta$ 1-42) was used in our investigation, and measurements of two-photon-excited fluorescence of the free and covalently conjugated peptide structure were carried out. The peptide secondary structure was correlated with a short fluorescence lifetime component, and this was associated with intramolecular interactions. Comparison of the fractional occupancy of the fluorescence lifetime measured at different excitation modes demonstrates the high sensitivity of the two-photon method in comparison to one-photon excitation (OPE). These results give strong justification for the development of fluorescence-lifetime-based multiphoton imaging and assays.

### Introduction

Protein misfolding is important to the conformational transition which facilitates the processes of protein aggregation.<sup>1</sup> Amyloid proteins undergo structural transitions leading to the appearance of amyloidogenic intermediates followed by aggregate formation.<sup>1</sup> The formation of soluble and protofibrillar aggregates composed of a small number of monomers constitutes the primary toxic species in several neurodegenerative disorders.<sup>2–5</sup> Oligomer toxicity appears to be related to a common conformational state, as shown by similar reactivity with conformation-dependent antibodies and comparable toxicity with oligomers synthesized from non-disease-related proteins and peptides.<sup>2,6,7</sup> These results suggest that different conformations of the amyloid peptides may contribute to the pathology via various mechanisms.<sup>8</sup> In the event of multiple conformational pathways of amyloid protein folding, the characterization of these conformations and the mechanisms involved in protein misfolding and aggregation are very important for identifying targets and designing inhibitors that could limit the toxicity of amyloid proteins.

Amyloid  $\beta$  peptide (A $\beta$ 1-42) is one of the major constituents of amyloid plaques found in the brains of Alzheimer's disease (AD) patients and is derived from a proteolytic process of the amyloid precursor protein (APP).<sup>9,10</sup> Direct observation of real-time conformational transitions in A $\beta$  is difficult due to its lack of solubility in water. Previous NMR studies on structural and conformational changes during monomer folding and assembly of A $\beta$  were conducted in acidic solutions,<sup>11</sup> organic solvents,<sup>12</sup> and a mixture of organic solvent with water.<sup>13</sup> Among the organic solvents utilized, hexafluoroisopropanol (HFIP) is very promising due to its tunable polarity properties.<sup>14</sup> This feature offers the opportunity to mimic membrane-induced conformational changes from monomers to the protofibrillar formation at concentrations suitable for NMR studies.<sup>15</sup> By controlling experimental conditions and utilizing several spectroscopic

techniques, such as circular dichroism (CD), Fourier transform infrared (FTIR), and nuclear magnetic resonance (NMR), assembly-dependent conformational changes of the A $\beta$  have been observed, including random coil  $\rightarrow$   $\beta$ -sheet,<sup>16–19</sup>  $\alpha$ -helix  $\rightarrow$   $\beta$ -sheet,<sup>19–22</sup> and random coil  $\rightarrow$   $\alpha$ -helix  $\rightarrow$   $\beta$ -sheet.<sup>23</sup> The components of the peptide sequences involved in these transitions are rather diverse,<sup>24–26</sup> however, and it is vital to know how particular subdomains direct conformational transitions and aggregation of the amyloid peptides at the molecular level. For example, the N-terminal domain of the A $\beta$ 1-42 contains a sequence that is not only critical for initiating  $\alpha$ - $\beta$  conformational switching,<sup>27,28</sup> but also essential for targeting antibodies<sup>29,30</sup> and compounds that alter A $\beta$  aggregation.<sup>31</sup> A detailed investigation of this domain motion (flexibility) within the A $\beta$ 1-42 at the residue level has not been reported. Therefore, it is urgent to establish a novel fluorescence-based method for measuring intramolecular interactions involved in this particular region. Such information will provide insights into the design of effective and preventative treatments for neurodegenerative diseases.

The conformational transition of the A $\beta$  has been extensively studied by pH changes, by alterations of environmental hydrophobicity, or through binding with other proteins.<sup>32–34</sup> Spectroscopic techniques such as NMR and CD have been used to gather a wealth of information on the conformational pathways of Alzheimer's peptides in aqueous media.<sup>13,15,34</sup> However, the limitations of these techniques have restricted their use. For example, the low sensitivity of NMR techniques requires high protein concentrations and as such the proteins tend to aggregate in their native states or change the natural structural conformations. Much attention should also be given to the relevance of NMR results (millimolar concentration) with the structural information obtained from CD spectroscopy (micromolar concentration). Furthermore, CD spectroscopy is not residue-specific, and hence cannot resolve the environmental effects at the residue level or measure the motional degrees of proteins and peptides. In contrast, the utility of fluorescence emission

\* Corresponding author. E-mail: tgoodson@umich.edu.

in studying protein motions and residue recognition has been realized due to its sensitivity, kinetic resolution, and compatibility with both living cells and physiological assays.<sup>35–39</sup> These features offer great opportunities in determining protein aggregates (biomarkers) at physiological conditions,<sup>35,36</sup> in residue-specific studies<sup>37,38</sup> and in optical imaging.<sup>39</sup> Presently, there have been no reports on the application of two-photon excitation (TPE) coupled with time-resolved fluorescence as a sensitive approach toward the studies of conformation and aggregation processes in amyloid peptides and proteins.

The use of fluorescence methods to probe the conformations and dynamics of proteins often requires the labeling of these biomolecules with an extrinsic fluorescent dye. Preservation of protein function and activity is a prerequisite for covalent attachment of fluorophores to a biomolecule. The vast majority of fluorescence labeled biopolymers (proteins and peptides) are achieved by labeling the common amino acids (lysine, glutamic acid, and arginine) found in proteins with widely available fluorescent probes. To closely interrogate the connection of the fluorescence dynamics of the probe to the conformation and motion dynamics of the proteins, several strategies including the reduction of flexible linkers between probes and proteins,<sup>40</sup> as well as the synthesis of environmentally sensitive near-infrared (NIR) chromophores, have been suggested.<sup>41</sup> To eliminate the conjugation effect on aggregation properties and to effectively couple the probe motion from the local and segmental motions<sup>42,43</sup> of the A $\beta$ 1-42, we used a system where 5-carboxytetramethylrhodamine (TAMRA) was conjugated at the N-terminus of the peptide to study fluorescence dynamics and subsequently correlate those properties with conformational changes and aggregation of A $\beta$ 1-42.

The significance of this investigation also lies in the recent interest in amyloid polymorphism,<sup>44</sup> highlighting the need to measure the conformations facilitating the aggregation processes under various conditions. Different cellular and tissue surroundings provide the environments that are likely to determine the particular amyloid structures,<sup>45,46</sup> so it is very important to develop methods and probes that can eventually be applied to A $\beta$  aggregates in cells and tissue samples. In this regard, nonlinear materials and optical approaches with particular emphasis on multiphoton-excited spectroscopy and microscopy enable more widespread and accessible detection platforms for both early diagnosis of the disease and evaluation of anti-A $\beta$  therapeutics.<sup>47,48</sup> In this contribution, we show that TPE coupled with time-resolved fluorescence spectroscopy is a promising technique to sensitively characterize conformational changes associated with aggregation of proteins and peptides. Accordingly, we suggest that TAMRA-labeled A $\beta$ 1-42 is a probe that may be used for monitoring protein conformational changes, a potential fluorescent marker for lifetime-based multiphoton imaging and assays, and a promising reporter for high-throughput assays.

## Experimental Section

**Chemicals.** 5-Carboxytetramethylrhodamine (TAMRA) and 1,1,1,3,3,3-hexafluoro-2-propanol (HFIP) were obtained from Molecular Probe and Sigma-Aldrich, respectively. Phosphate buffered saline (PBS, catalog no. P312-500, pH 7.4, without Ca or Mg) was received from Invitrogen Corporation. Sodium azide (NaN<sub>3</sub>) was obtained from Fluka. Synthetic TAMRA-labeled A $\beta$ 1-42 (lot 39003, HPLC purity >90%) and A $\beta$ 1-42 (lot 44103, HPLC purity >95%) were purchased from AnaSpec Inc. (San Jose, CA). All chemicals and peptides were used without further purification as obtained from the manufacturer.

Unless specified, a PBS buffer prepared containing 211 ppm NaN<sub>3</sub> was used in the preparations of HFIP/PBS solutions.

**A $\beta$  Sample Preparation.** To disaggregate the A $\beta$  and generate monomeric  $\alpha$ -helical structures, a stock solution of the TAMRA-A $\beta$ 1-42 was prepared by dissolving 0.1 mg of this peptide into 100  $\mu$ L of HFIP and was then stored in the refrigerator ( $-20$  °C) until use. The concentration of this stock solution was estimated by measuring the optical absorption at 547 nm (extinction  $\epsilon = 7.3 \times 10^4$  M<sup>-1</sup> cm<sup>-1</sup> for 5-TAMRA in neat HFIP). A stock solution of the A $\beta$ 1-42 was also prepared by dissolving 1 mg of this peptide into 445  $\mu$ L of HFIP and then subsequently stored in the refrigerator ( $-20$  °C) before use. For concentration-dependent aggregation measurements, peptide samples of various concentrations were prepared by dilution from the stock solution and maintained in a cosolvent of HFIP/PBS (20:80). These solutions were then stored in the dark at room temperature.

**Steady-State Measurements.** All CD spectra were recorded with an Aviv Model 202 circular dichroism spectrometer at 25 °C using a bandwidth of 1.0 nm and a wavelength step of 0.5 nm. A quartz cell with an optical path of 0.1 cm was used for far-UV (190–240 nm) measurements. Estimation of the percentage of  $\beta$ -sheet,  $\alpha$ -helix, and random coil was made using a K2D program.<sup>49,50</sup> In the case of a negligible contribution of  $\beta$ -sheet, the percentage of  $\alpha$ -helical content was estimated using the following equations for ellipticities at 208 and 222 nm:<sup>51,52</sup>

$$\alpha\text{-helix } (\%)_{208\text{ nm}} = \frac{\theta_{208} - 4000}{-33000 - 4000} \times 100$$

$$\alpha\text{-helix } (\%)_{222\text{ nm}} = \frac{\theta_{222} - 3000}{-36000 - 3000} \times 100$$

where  $\theta$  is the mean residue ellipticity in units of deg cm<sup>2</sup> dmol<sup>-1</sup>.

Unless specified, absorption and fluorescence spectra were recorded on an Agilent (Model 8341) spectrophotometer and Fluoromax-2 fluorimeter (ISA instruments New Jersey), respectively. Measurements were performed using a 45  $\mu$ L quartz cell with an optical path of 0.3 cm at room temperature. Emission spectra were collected at increments of 1 nm over the range  $\lambda_{\text{em}} = 550\text{--}700$  nm ( $\lambda_{\text{ex}} = 535$  nm) for both the free dye and the dye-labeled peptide. The two-photon-absorption cross sections ( $\delta$ ) of all samples were measured by the two-photon induced fluorescence method.<sup>53</sup> These measurements have been described in detail elsewhere.<sup>54</sup> Fluorescence quantum yields ( $\phi$ ) were measured using a known procedure.<sup>55</sup> The integrated fluorescence intensity from the sample was compared with that for the standard dye Rhodamine B in methanol.

**Two-Photon-Excited Fluorescence Lifetime and Polarization Measurements.** Two-photon-excited time-resolved fluorescence measurements were carried out by time-correlated single photon counting (TCSPC) with two-photon excitation (TPE). The TCSPC system has been described in detail elsewhere.<sup>56</sup> The excitation source was a Kapteyn Murnane Laboratories (KML) mode-locked Ti:sapphire laser system delivering  $\sim 30$ -fs output pulses at 800 nm at a repetition rate of 90 MHz. The average excitation power at the sample was near 10 mW. The absorption spectra and the reproducibility of the fluorescence dynamics in the course of the experiment were monitored to make sure that the sample was stable. No photodegradation of the sample has been detected at this power level. For one-photon excitation (OPE) the laser frequency  $\sim 800$

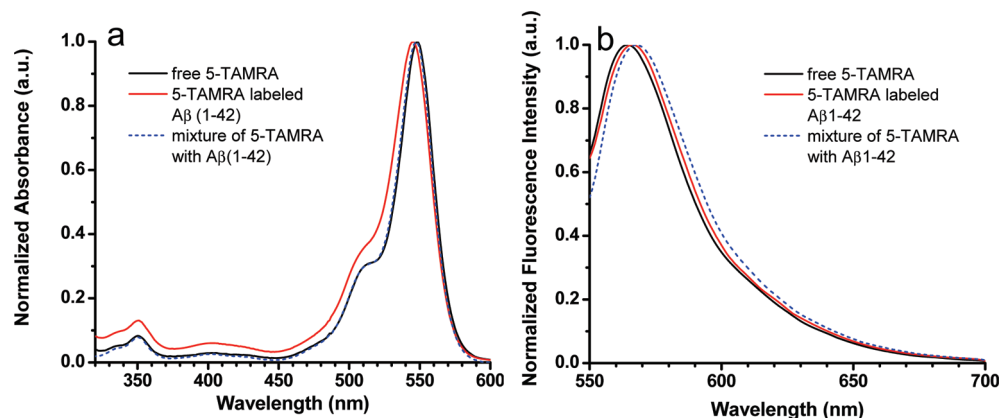


**Figure 1.** (a) Absorption spectra normalized at the maximum absorption peak. (b) Normalized emission spectra of the chromophore– $A\beta$ 1-42 systems. Samples were prepared to have a concentration of 15  $\mu$ M in HFIP.

nm laser output was frequency doubled in a nonlinear crystal to generate excitation pulses at  $\sim$ 400 nm. The excitation beam for either 400 or 800 nm excitation routes was focused on the sample in a 45  $\mu$ L quartz cell using a lens with a focal length of 9 cm. The fluorescence was taken at a right angle to the excitation and detected by a PMT (photomultiplier tube) module mounted at the exit slit of a monochromator (Thermo Oriol 77250). A TimeHarp 200 (PicoQuant) detection card was used for time-correlated single photon counting measurements. For fluorescence decay measurements a prism polarizer was oriented at a magic angle ( $54.70^\circ$ ) relative to the vertical polarization of the excitation beam. Fluorescence anisotropy decay measurements were carried out by recording the fluorescence with the polarizer oriented either parallel or perpendicular with respect to the excitation polarization. For TPE, the instrumental response function (IRF) was recorded using a Rayleigh scattering medium prepared by mixing colloidal gold nanoparticles with a few drops of 6 M NaCl.<sup>57</sup> The time profile of the fluorescence was analyzed and fitted to the model decay function using PicoQuant Fluofit software including deconvolution with the IRF. The goodness of the fitting of time-resolved decay profiles was evaluated by  $\chi^2$ .

## Results and Discussion

**Circular Dichroism.** In order to establish an understanding of the initial conformation of the TAMRA-labeled  $A\beta$ 1-42 peptide and to make correlations with fluorescence lifetimes, circular dichroism spectroscopy was used to analyze the secondary structure of these systems. Previous reports have shown the relative structural heterogeneity in the residues 1–17 of  $A\beta$ 1-42,<sup>58,59</sup> so determination as to whether labeling the N-terminus of  $A\beta$ 1-42 significantly alters the structural characteristics of the unlabeled peptide is critical for our studies as the chromophore should not influence the peptide interactions.<sup>58</sup>

The approximate fraction of  $\alpha$ -helix secondary structure was determined for the unlabeled peptide and compared to that obtained from the labeled peptide in neat hexafluoroisopropanol. The percentage of  $\alpha$ -helix for each sample was found to be the same within experimental uncertainties, and any residual random coil structure remained similar between systems. This indicates that labeling with TAMRA at the N-terminus does not appreciably change the structural nature of the  $A\beta$ 1-42 over the concentration ranges of interest. Other recent reports<sup>60–62</sup> using various biochemical techniques including CD spectroscopy seem to corroborate this finding, as Bateman<sup>62</sup> observed that similarly labeled  $A\beta$  showed no structural differences compared to that

of the unlabeled peptide. The structural information gathered from the TAMRA-labeled  $A\beta$ 1-42 would therefore reflect those properties such as conformational changes and aggregation of the native peptide.

**Steady-State Spectroscopy.** To further analyze whether the attachment of TAMRA to  $A\beta$ 1-42 significantly altered the behavior of the native peptide, the absorption and emission spectra were obtained for the TAMRA-labeled  $A\beta$ 1-42, the unattached TAMRA chromophore, and a mixture of unlabeled  $A\beta$ 1-42 with the unattached chromophore. Figure 1 shows the absorption and emission spectra obtained for each system as prepared in neat HFIP. The absorption spectrum of the dye-labeled peptide shows an absorbance maximum at 545 nm which is slightly blue shifted compared with TAMRA. Similarly, the emission spectra show a progressive red shift from the free-TAMRA ( $\lambda_{\max} = 564$  nm), to the TAMRA-labeled  $A\beta$ 1-42 ( $\lambda_{\max} = 566$  nm), and to the mixture of TAMRA with  $A\beta$ 1-42 ( $\lambda_{\max} = 568$  nm). The emission spectrum of the labeled peptide does not exhibit a typical mirror-image relationship with the absorption spectrum, notably showing only a small red-shifted emission resulting from the excitation of the 545 nm band. These small shifts can be attributed to either some small aggregates of rhodamine dyes<sup>63</sup> forming ground-state complexes or to interactions between certain amino acid side groups of  $A\beta$ 1-42 and TAMRA<sup>64</sup> causing a slight bathochromic shift.

A comparison of the absorption spectra for free TAMRA and the mixture of free chromophore and unlabeled  $A\beta$ 1-42 notably demonstrates the absence of ground-state complexes being formed in the mixture where the dye is not covalently conjugated to the peptide. This indicates that any interactions that may be occurring in TAMRA-labeled  $A\beta$ 1-42 are resulting from the covalently attached chromophore and not from interactions between free dye molecules. With respect to the free-TAMRA system, this feature also suggests that any ground-state interactions that may be occurring are too weak to shift the maximum absorption peak. The noticeably blue-shifted absorption spectrum of the TAMRA-labeled  $A\beta$ 1-42 could be a consequence of intermolecular complexes formed among the covalently conjugated TAMRA as was observed previously in a polypeptide system labeled with 5',6'-carboxytetramethylrhodamine probes that aggregated into H-type dimers.<sup>65</sup>

Figure 2 depicts a schematic representation of possible aggregation and peptide–TAMRA interactions for TAMRA-labeled  $A\beta$ 1-42. These may include the fluorescence quenching of TAMRA by intramolecular interactions with certain amino acids (as described below) or the formation of a ground-state

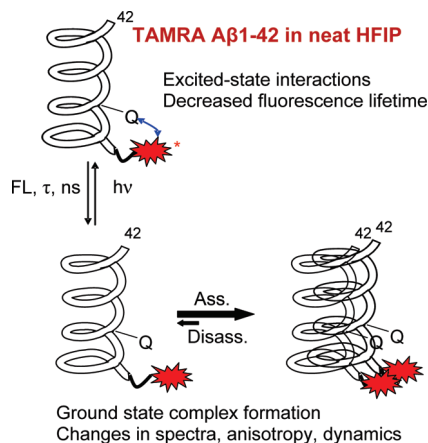


**Figure 2.** Schematic representation of conjugation effects and structural conformation of TAMRA-labeled A $\beta$ 1-42 in neat HFIP.

complex between two TAMRA molecules. It should be noted that the peptide concentration (15  $\mu$ M) utilized in our steady-state measurements is lower than the concentrations generally required for the formation of ground-state complexes among free rhodamine chromophores.<sup>63</sup> However, since TAMRA is covalently conjugated to the peptide, the dye is constrained to the N-terminus of the A $\beta$ 1-42. As a result, the effective local concentration of the covalently conjugated TAMRA in the immediate vicinity of a particular region of the peptide may be high enough to bring the chromophores into close proximity, leading to ground-state complex formation. The blue-shifted absorption maximum may suggest the formation of H-type aggregate geometry with a parallel or side-by-side alignment of the two covalently conjugated TAMRA chromophores.<sup>65</sup> However, it is clear that the steady-state spectroscopy does not afford the ability to definitively confirm the types of aggregates being formed in solution and does not provide information as to the peptide secondary structure. Time-resolved fluorescence lifetime and anisotropy measurements should permit more definitive conclusions to be drawn as to the charge interactions taking place and types of aggregates formed.

**Two-Photon Absorption (TPA).** Before we measured the two-photon-excited fluorescence of the conjugated peptide, the two-photon response of the TAMRA chromophore was investigated. The TPA excitation spectra for rhodamines typically have a substantial peak around 820 nm<sup>66</sup> and initial anisotropy values that are very high, reaching as high as  $r_0 = 0.5$  for Rhodamine 6G.<sup>66,67</sup> This makes rhodamine derivatives including TAMRA attractive probes for TPA excitation around 800 nm where robust and flexible Ti:sapphire laser sources of femto-second light pulses are available.

The excitation power dependence of the TAMRA fluorescence detected at 565 nm was determined by a log–log plot of the fluorescence signal versus incident peak photon flux at  $\sim$ 800 nm. For photon flux densities  $\leq 6.0 \times 10^{26}$  photons  $\text{cm}^{-2} \text{s}^{-1}$ , the induced fluorescence obeyed a quadratic intensity dependence as indicated by a measured slope of 2.0, thereby confirming the dominance of the TPA excitation route at this wavelength. TPA cross sections at 800 nm were measured for the dye-labeled A $\beta$ 1-42 and free dye using the two-photon-excited fluorescence method. The cross sections ( $\delta$ ) for the TAMRA and TAMRA-labeled A $\beta$ 1-42 in pure HFIP were found to have relatively large TPA cross sections similar to those of comparable rhodamine chromophores.<sup>66</sup> The free-TAMRA chromophore was found to have a TPA  $\delta = 185$  GM and the peptide-conjugated TAMRA had a larger cross section of 313

GM (Table 1). The increase in cross section can be rationalized due to differences in dipole moment of the chromophore when it is attached to the peptide versus unattached in solution and due to the possible intermolecular interactions of the labeled peptide molecules in solution as illustrated in Figure 2. This enhanced cross section of the TAMRA-labeled A $\beta$ 1-42 is advantageous for our studies using time-resolved fluorescence lifetimes and anisotropy as it permits easier signal detection and increased sensitivity to aggregates.

Comparing the TPA excitation route with OPA, two-photon absorption at 800 nm excites the molecule well above the lowest energy level ( $S_1$ ) located at 545 nm (Figure 1a). Due to the ultrafast (femtosecond) internal conversion of the TPA state to the relaxed fluorescence state, the fluorescence originates from the same state as for resonant OPA excitation. At 400 nm, the OPA is essentially nonresonant. The respective initial anisotropies for 400 nm are quite low for rhodamines ( $r_0 < 0.1$ ) as excitation to the higher state ( $S_2$ ) located at 350 nm also takes place at this wavelength.<sup>68,69</sup> The excitation route via  $S_2$  leads to a negative contribution to the anisotropy, while the excitation to the  $S_1$  produces fluorescence with positive anisotropy.<sup>69</sup> The combination of these two contributions produces very low total initial anisotropy, making accurate measurement of orientational dynamics for this excitation regime very difficult.

**Fluorescence Lifetime Measurements.** Fluorescence emission with two-photon excitation is particularly interesting as it gives a more specific signature regarding conformational changes of proteins and peptides than the emission detected using one-photon excitation. By utilizing the promising TPEF decay time technique, efforts were made to investigate conformational changes and molecular interactions of the amyloid peptides. To apply the unique TPE-TCSPC technique to the structural characterization of A $\beta$ 1-42, fluorescence decays of a 15  $\mu$ M dye-labeled A $\beta$  in a solvent of HFIP/PBS (20:80) were measured. As shown in Figure 3, the excited-state population decays of the covalently conjugated TAMRA were fitted with a two-component exponential decay function and the fluorescence lifetimes were found to be  $0.4 \pm 0.1$  ns (36%) and  $3.4 \pm 0.2$  ns (64%), respectively. This differs from the excited-state population decay of the free dye measured under the same conditions which gives only a single fluorescence lifetime ( $4.08 \pm 0.05$  ns), in agreement with the first-order dynamics that have been reported in the literature.<sup>70</sup> This discrepancy between the dynamics of the free and covalently conjugated TAMRA has significant implications on the application of its photophysical properties to the study of amyloid peptide structures and their molecular interactions. The labeled N-terminus of the peptide is likely interacting with other amino acids found in the peptide, resulting in fluorescence quenching and the appearance of a shorter lifetime decay component not seen in the free dye system. If we could identify the particular A $\beta$ 1-42 conformation that permits this interaction, then fluorescence lifetimes may provide insight into the larger secondary structure of the peptide.

Previous investigations on the molecular interactions of TAMRA-labeled macromolecules suggest the existence of various conformational states of TAMRA, each with distinct fluorescence lifetimes.<sup>55,71–73</sup> Depending upon the techniques utilized in these investigations, the number of conformational states and fluorescence lifetimes could vary among the different systems.<sup>55,73</sup> However, two major conformational states of the covalently conjugated TAMRA have been observed in all systems.<sup>55,71–73</sup> One (type A) occurs when the dye molecule is close in proximity to a quenching site, and the other (type B) occurs when the chromophore is far removed from quenching

**TABLE 1: Summary of Linear and Nonlinear Optical Properties of TAMRA-Labeled A $\beta$ 1-42 and TAMRA Free Chromophore**

	$\lambda_{\max}$ (nm)		fluorescence lifetime (ns)		$\eta$	$\delta$ (GM) <sup>c</sup>	$\eta\delta$ (GM) <sup>c</sup>
	abs <sup>d</sup>	em <sup>c</sup>	short <sup>d</sup>	long <sup>d</sup>			
labeled A $\beta$ 1-42 <sup>a</sup>	545	566	0.4 $\pm$ 0.1	4.5 $\pm$ 0.3	0.61	313	191
free TAMRA <sup>b</sup>	548	564	NA	4.07 $\pm$ 0.05	0.75	185	139

<sup>a</sup> Prepared concentration of 19  $\mu$ M. <sup>b</sup> Prepared concentration of 20  $\mu$ M. <sup>c</sup> Solution 100% HFIP. <sup>d</sup> Solution HFIP:PBS (30:70).

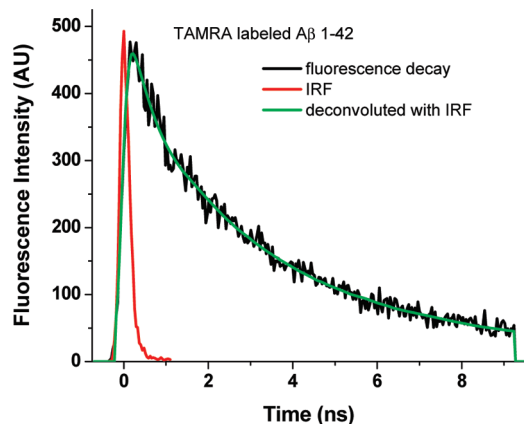


**Figure 3.** Typical TCSPC decay trace of TAMRA-labeled A $\beta$ 1-42. TAMRA-labeled A $\beta$ 1-42 (15  $\mu$ M) was incubated in HFIP/PBS (20:80) for 2 weeks prior to measurements.

sites. The molecules with type A conformations have picosecond (“ps”) fluorescence lifetimes with low quantum yields due to photoinduced electron transfer (PET) reactions.<sup>71–76</sup> Molecules with type B conformations have long decay fluorescence lifetimes (several nanoseconds) and high quantum yields (since there is no PET), and are more associated with the solvent environment.<sup>74,75</sup> Since the two-component fluorescence decays obtained from the TAMRA-labeled A $\beta$ 1-42 system are similar to those decays observed in TAMRA–DNA<sup>55,71–73</sup> and TAMRA–peptide<sup>64</sup> conjugated systems, it can be inferred that both type A and B conformations of the conjugated TAMRA may be present in our peptide system. Consequently, the short decay component would reflect the interactions of the covalently conjugated TAMRA with amino acid quenchers constituted in the A $\beta$ 1-42, while the long decay component reveals solvent-related environmental changes in relation to the chromophore.

In reviewing the amino acid sequence in the A $\beta$ 1-42, the potential fluorescence quenchers are methionine and histidine as well as the aromatic amino acids tyrosine and phenylalanine. Previous investigations on fluorescence quenching of TAMRA by these amino acids have demonstrated that tyrosine is the most pronounced fluorescence quencher.<sup>64</sup> By working at sufficiently low peptide concentrations (micromolar), a tyrosine residue in A $\beta$ 1-42 at sequence position 10 could serve as an efficient electron acceptor for a two-photon induced electron transfer (2PET) reaction. NMR analysis of the structural ensembles of A $\beta$ 1-42 in HFIP/water (30:70) has shown that most  $\alpha$ -helical structure corresponds to the amino acid sequence in the 10–23 region.<sup>13</sup> This result provides insight into tyrosine behavior when the peptide is dissolved in HFIP/PBS (20:80) to induce the formation of more ordered conformations and aggregates.

As shown in Figure 4, the N-terminus of A $\beta$ 1-42 is part of a flexible sequence of amino acid residues not prone to forming a larger secondary structure such as  $\alpha$ -helix or  $\beta$ -sheet. Therefore, the labeled N-terminus has the flexibility to adopt conformations in which the chromophore may interact with nearby amino acids such as tyrosine. As illustrated in Figure 4, the tyrosine located at position 10 is accessible for close contact

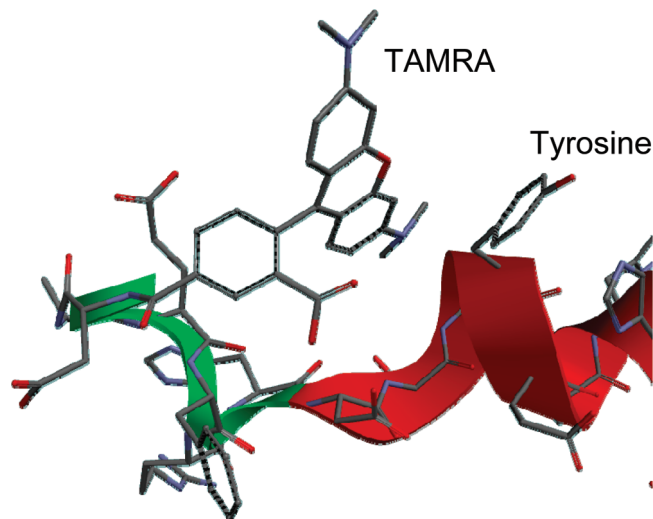


**Figure 4.** Interaction between TAMRA chromophore and tyrosine molecule at position 10. Under certain conditions, labeled A $\beta$ 1-42 may be present in conformations conducive for close intramolecular contact between TAMRA and the tyrosine residue at sequence position 10, resulting in fluorescence quenching and the short picosecond fluorescence lifetime.

with TAMRA under certain conditions in which the peptide is structured, allowing for the possibility of charge transfer between the two residues. In probing this connection by measuring 2PET-based fluorescence methods, it becomes possible to correlate the fluorescence lifetimes associated with this interaction with the basic conformational state of the peptide.

The connection between the fluorescence lifetimes and molecular interactions associated with the secondary structure was established by characterizing the secondary structures of the dye-labeled peptide at different concentrations using CD measurements and the short-time component fluorescence lifetimes obtained using TCSPC. An estimation of the secondary structural content versus peptide concentration is shown in Figure 5. After incubation of the peptides in HFIP/PBS (20:80) for 2 weeks, all peptides are predominantly in a random coil structure. However, the relative proportions of random coil,  $\alpha$ -helix, and  $\beta$ -sheet are concentration dependent due to the coexistence of equilibria among these composites. As can be seen from Figure 5, the amount of  $\alpha$ -helix structure increases with a decrease in random coil, and similar  $\beta$ -sheet content is retained as the peptide concentration increases from 6 to 9  $\mu$ M. These results indicate that, at such low concentrations, peptide interactions are probably important for stabilization and formation of  $\alpha$ -helical conformations, but not important for formation of  $\beta$ -sheet conformations. However, at peptide concentrations over 9  $\mu$ M, there is seen a rapid increase in the percentage of  $\beta$ -sheet structure coincident with a large decrease in random coil content. This result implies that at high peptide concentrations the conformational transition from random coil to  $\beta$ -sheet is due to increased intermolecular hydrophobic interactions and not through intramolecular interactions.<sup>12</sup>

**2PET-Based Fluorescence Quenching Model.** To correlate 2PET-based fluorescence quenching with peptide conformational

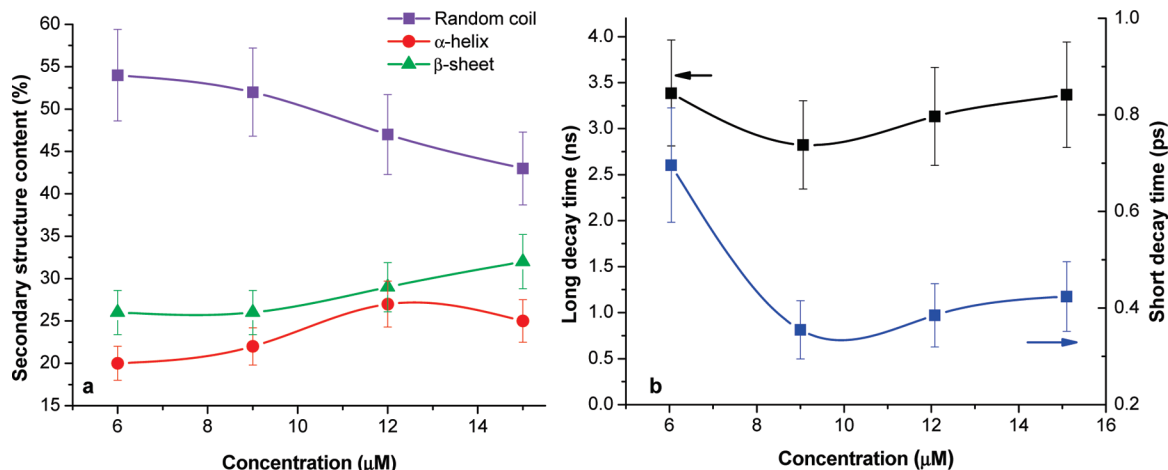


**Figure 5.** (a) Percentages of random coil,  $\alpha$ -helix, and  $\beta$ -sheet as a function of peptide concentration. (b) Concentration-dependent nanosecond fluorescence lifetime and the 2PET-based fluorescence decay time of the covalently conjugated TAMRA. All peptide samples were incubated with HFIP/PBS (20:80) solvent composites for 2 weeks prior to the measurements.

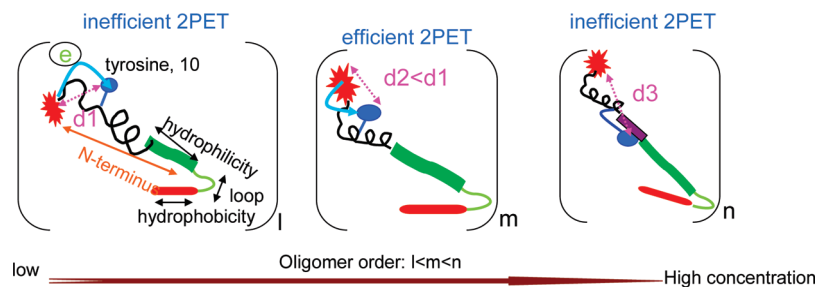


**Figure 6.** Model for description of intramolecular interaction between the covalently conjugated TAMRA and the tyrosine residue within  $A\beta_{1-42}$ . Due to the flexibility of the N-terminus, the concentration-dependent conformational changes bring the TAMRA close to tyrosine, yielding efficient 2PET-based fluorescence quenching.

changes involving intramolecular interactions between the TAMRA label and tyrosine residue, the absence of intermolecular charge transfer fluorescence quenching at these low peptide concentrations is assumed. Based on this assumption, the “picosecond” (short decay time) fluorescence dynamics relates information about the interaction between a tyrosine residue and the electronically excited TAMRA.<sup>64,77</sup> The correlation of concentration-dependent picosecond fluorescence decay time with secondary structural composites and consequently with conformational flexibility of the N-terminus of the peptides is also shown in Figure 5. To better understand this correlation, we present a schematic model for description of conformation in an associated distance-dependent 2PET process (Figure 6).

At a low peptide concentration, the peptide is characterized by a high percentage of random coil structure giving rise to the small degree of fluorescence quenching, i.e., “picosecond” fluorescence lifetimes on the order of 700 ps. This may take place when the tyrosine residue is trapped within a groove of the random coil which keeps the covalently conjugated TAMRA far away from the tyrosine residue, possibly at a large contact distance ( $>1$  nm).<sup>78</sup> At an intermediate peptide concentration, the peptide is less flexible and is characterized by more ordered structure (increased  $\alpha$ -helix content), which reduces the contact distance between TAMRA and tyrosine residue (Figure 4), leading to efficient intramolecular charge transfer fluorescence quenching indicated by faster fluorescence decays. At higher peptide concentrations (for example, over  $9 \mu\text{M}$ ), the flexibility of the N-terminus decreases due to a rapid increase in  $\beta$ -sheet content and decrease in random coil. The peptides with such secondary structures may lead the tyrosine to be buried within

the “hydrophobic pocket”. As a result, the 2PET-based fluorescence quenching is inefficient, leading the “picosecond” decay time to increase as peptide concentrations are increased from 9 to  $15 \mu\text{M}$ .

The long-lived fluorescence component originating from conformational state B of the conjugated TAMRA (away from quencher sites) reveals environmental changes associated with  $A\beta$  aggregation also critical to understanding the overall process. A clear assignment of fluorescence lifetimes to specific substances is impossible due to the heterogeneities of  $A\beta$  systems as well as the absence of a comprehensive theory relating excited-state lifetime to either local environment or molecular properties for systems whose emission bands experience significant inhomogeneous broadening. However, the measurement of excited-state lifetime can aid in understanding the impact of environmental factors, such as concentration, on fluorescence lifetime. The “nanosecond” fluorescence decay is predominantly associated with these and reports such factors as solvent accessibility<sup>83</sup> and peptide aggregation-induced chromophoric interactions.<sup>36</sup> Figure 5b displays the “nanosecond” fluorescence lifetime as a function of peptide concentration. A monotonic decrease in the nanosecond (ns) fluorescence lifetime is observed as the peptide concentration increases from 6 to  $9 \mu\text{M}$ . At these concentrations, a decrease in random coil parallel with an increase in  $\alpha$ -helix content (Figure 5a) suggests that ordered structures are formed through peptide–peptide interactions, leading the covalently conjugated TAMRA to be more solvent accessible. As a result, the fluorescence lifetimes decrease with an increase in peptide concentration from 6 to  $9 \mu\text{M}$ . However, when peptide concentration is over  $9 \mu\text{M}$ , a monotonic increase in the long-lived fluorescence lifetime is observed. CD analysis

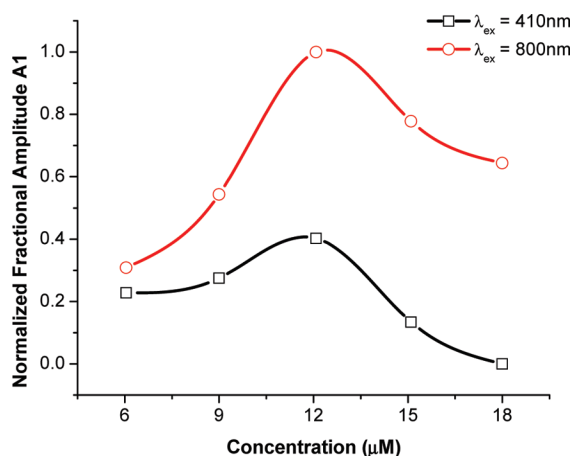


**Figure 7.** Comparison of excitation sensitivity and effect of peptide concentration on fractional occupancy A1 of the “picosecond” lifetime.

indicates that interactions among the peptides result in an increased aggregation rate and  $\beta$ -sheet. These interactions yield large aggregates, making it likely that the covalently conjugated TAMRA becomes trapped inside the aggregates with less solvent accessibility than at lower concentrations. By observing the change in fluorescence decay times measured with respect to solvent accessibility of the TAMRA label, the suggestion is furthered that the peptide aggregates formed at low concentrations differ from those formed at high concentrations. From these results, we conclude that intra- and intermolecular interactions lend 2PET-based fluorescence to the study of the conformational flexibility of the N-terminus in  $A\beta$  with residue-specific assays. This ability to correlate the peptide conformational state with its fluorescence lifetime at low concentrations opens a new avenue toward the measurement of  $A\beta$  conformational fluctuation at the signal molecular level unachievable with other predominately used techniques such as CD spectroscopy.

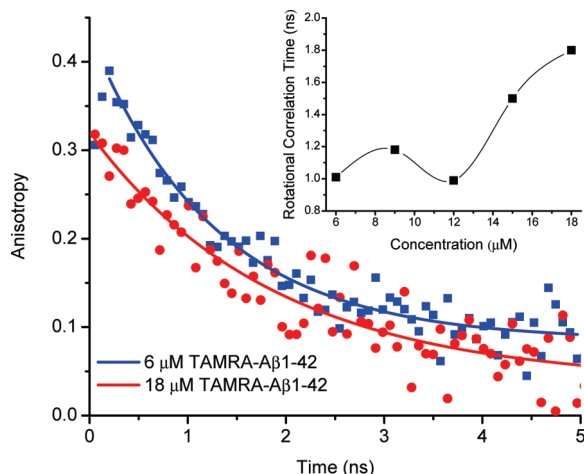
**Distribution of Conformational States from Fluorescence Lifetimes.** The concentration-dependent peptide interactions (aggregation) not only affect fluorescence lifetimes, but also influence the distribution of conformational states (A and B) of the covalently conjugated TAMRA. Figure 7 shows the fractional occupancy (amplitude) A1 of the “picosecond” decay lifetime as a function of peptide concentration. As seen from this figure, there is an initial increase in A1 as the peptide concentration is varied from 6 to 12  $\mu\text{M}$  followed by a decrease as the concentration is further increased to 18  $\mu\text{M}$ . At low peptide concentrations, the structures of the peptides are flexible, an indication of a larger percentage of random coil. In this case, intramolecular contact between tyrosine and TAMRA becomes more feasible, giving rise to a larger distribution of the short decay component A1. However, at higher peptide concentrations, the rate of peptide aggregation increases to form large aggregates with increased  $\beta$ -sheet content. The greater structural content of these peptides prevents the covalently conjugated TAMRA from having fluorescence quenching interactions, resulting in smaller values for amplitude A1. These results when analyzed in conjunction with the concentration-dependent fluorescence lifetimes provide a clear picture as to the conformational flexibility of amyloid peptides over a range of concentrations while also giving an indication as to the types of intra/intermolecular interactions influencing these conformational states.

Figure 7 also compares the sensitivity to the mode of excitation of the fractional occupancy A1 of the covalently

conjugated TAMRA. The fractional occupancy A1 obtained from the two-photon-excited fluorescence lifetimes is much larger than that determined from OPE. The heterogeneities of a given peptide may lead to a wide range of excited states to which the excitation is sensitive and selective. As demonstrated previously, the emitting molecule with type A conformation emerges from the case where the covalently conjugated TAMRA is situated in the vicinity of tyrosine (Figure 4). This intramolecular contact induces the excited TAMRA–tyrosine to have charge transfer character that is associated with concentration-dependent peptide conformations. While TAMRA molecules with type B conformations are photophysically unaffected by tyrosine due to the large distance separation between them, the fluorescence decay times arising from such conformations may reflect the effects of intermolecular interactions caused by peptide aggregation. Since TPE is a nonlinear process and strongly affected by the charge transfer character of the molecule,<sup>55</sup> the two-photon absorption cross section is expected to be large for the molecules with type A conformations over type B, thus differentiating TPE from OPE, which cannot discriminate between the two types. Two-photon excitation could therefore permit the monitoring of larger population decays from molecules with type A conformation more easily than OPE (Figure 6), the primary implication being that TPE predominates the distribution of excited-state molecules relating to the amount of charge transfer. This additional specificity makes it advantageous over OPE because with inhomogeneous systems such as  $A\beta$ 1-42 many different conformations and aggregates are coexisting at the same time, so the ability to selectively monitor a particular conformation or aggregate is vitally important to being able to completely understand the system.

**Two-Photon-Excited Depolarization.** Two-photon-excited time-resolved fluorescence anisotropy (TPE-TRFA) takes advantage of the large fluorescence dynamic range permitted which is particularly beneficial to the determination of rotational correlation times greater than the fluorescence lifetimes.<sup>58</sup> While the essential physics of molecular motion is independent of the excitation mechanism, the means by which the initial anisotropic distribution is excited can provide more detailed and complementary information on a molecular motion.<sup>79</sup> In particular, the initial fluorescence anisotropy for TPA excitation (0.57) is substantially higher than that for OPE (0.4), which is potentially very useful for resolving complex rotational kinetics with multiple rotational correlation times and restricted rotation.<sup>69,80</sup> Additionally, it has been found that the TPE initial anisotropy is nearly independent of the excitation wavelength,<sup>81</sup> allowing for use of a larger variety of probes at a particular excitation wavelength or a broader choice of excitation wavelengths for a specific probe.

The conjugated TAMRA located on the N-terminus of the  $A\beta$ 1-42 is unable to sense the true dynamics at the C-terminus due to the relatively long separation provided by the hydrophobic core of the  $A\beta$ . TPE-TRFA studies on the conjugated TAMRA were used to detect the local motion of the random side chain to which the probe is covalently attached or the motion of short  $A\beta$ 1-42 segments. Table 2 lists the two-photon-excited fluorescence anisotropic decays measured at different peptide concentrations. All decays were successfully deconvoluted into a single rotational correlation time. Systematic decreases in both the rate of motion and initial value of fluorescence anisotropy are observed when the peptide concentration increases from 12 to 18  $\mu\text{M}$ .



**Figure 8.** Time-resolved fluorescence anisotropy lifetimes of 6 and 18  $\mu\text{M}$  TAMRA-labeled  $A\beta_{1-42}$ . Inset shows rotational correlation time as a function of concentration.

**TABLE 2: Rotational Anisotropy Decay Parameters for TAMRA- $A\beta_{1-42}$  Dissolved in HFIP/PBS (20:80)**

concn ( $\mu\text{M}$ )	$\tau$ (ns)	$r_0$
6	$1.01 \pm 0.07$	0.36
9	$1.18 \pm 0.09$	0.29
12	$0.99 \pm 0.07$	0.35
15	$1.5 \pm 0.2$	0.33
18	$1.8 \pm 0.4$	0.29

The anisotropic fluorescence decay of the conjugated TAMRA is complicated due to the heterogeneous nature of our system. It is difficult to attribute our single-exponential anisotropic decay to specific conformational states as was done with the previously measured multicomponent fluorescence lifetimes. However, the concentration dependence of the orientational dynamics of the covalently conjugated TAMRA may reveal local motions associated with the packing state of the peptides. This packing is clearly evidenced by the increased rotational correlation times ( $\tau$ ) of the chromophore as the concentration of the peptide is increased, an indication of the growing size of the aggregates. As shown in Figure 8, at peptide concentrations ranging from 6 to 12  $\mu\text{M}$ , the rotational correlation times of the covalently conjugated TAMRA are slightly longer than the local motion of the free dye ( $700 \pm 50$  ps) under the same conditions. This implies that there is more restricted movement of the covalently conjugated TAMRA. Closer relative intermolecular packing of the chromophores and weak coupling of the TAMRA to the orientational dynamics of the peptide N-terminus explain the longer correlation times, much the way it has been observed in a TAMRA-labeled DNA system.<sup>82</sup> As the peptide concentrations are increased from 12 to 18  $\mu\text{M}$ , the rate of depolarization of the covalently conjugated TAMRA becomes more than 2 times slower than that of the free dye. The measured slower decays are evidence of the fact that, as more compacted conformations (or aggregates) begin to dominate the system at higher concentrations (Figure 5), the motion of the TAMRA probe becomes increasingly hindered.

## Conclusions

The sensitive approach of coupling two-photon emission with time-resolved fluorescence and fluorescence anisotropy was applied to study the conformational changes and early aggregation of amyloid peptides. The characterization of these early aggregates may lead to important discoveries allowing for the

prevention or treatment of neurodegenerative diseases, but research into these early stages of aggregation has been hindered by the limitations of other techniques. It remains critical though to understand these early forms as they may be indicative of the pathway leading to the formation of toxic amyloid fibrils. By labeling  $A\beta_{1-42}$  with TAMRA, we were able to probe the conformational flexibility of the peptide by detecting intramolecular, residue-specific interactions involving our chromophore and a tyrosine residue in the peptide (Figure 4). Using the short fluorescence lifetime of the labeled peptide and conformational measurements performed using circular dichroism spectroscopy, the secondary structure of the peptide was able to be correlated to specific fluorescence lifetimes (Figure 5), thereby permitting the study of conformational changes in amyloid peptides at the residue level, something not able to be achieved with more commonly used techniques. Fluorescence anisotropy measurements demonstrate that two-photon excitation allows for enhanced selectivity and sensitivity for aggregating peptides, especially for those conformations exhibiting short fluorescence lifetimes and strong charge transfer interactions between chromophore and residue. These depolarization results differ significantly compared with those obtained from typical one-photon excitation (Figure 7) which show far lower amplitude for the same systems. The anisotropic decays and fluorescence lifetimes together provide a clear picture as to the conformational flexibility of amyloid peptides over a range of concentrations (6–18  $\mu\text{M}$ ) while also giving an indication as to the types of intra/intermolecular interactions influencing these conformational states.

The ability to monitor the fluorescence dynamics (lifetimes and anisotropy) of the covalently conjugated TAMRA as a function of aggregation and secondary structural changes of the  $A\beta$  provides a valuable tool for the characterization of conformation and molecular interactions of the amyloid peptides even at low concentrations. Our findings have implications in the utilization of fluorescence methods to measure and image  $A\beta$  conformational fluctuation at the signal molecular level and in the detection of small neurotoxic aggregates formed at low peptide concentrations. The high sensitivity of TPE to peptide structural changes offers the possibility to quantitatively monitor the early aggregation of the  $A\beta$  at physiological conditions. A promising application of these decay time techniques using the TAMRA-labeled peptide is in the detection of early aggregates of amyloid proteins via multiphoton fluorescence lifetime imaging and lifetime-based assays.

**Acknowledgment.** The authors thank the Army Research Office and the National Science Foundation for support.

**Supporting Information Available:** Figures S1 and S2 showing initial CD spectroscopy of labeled and unlabeled  $A\beta$  in neat HFIP and CD spectra collected as a function of peptide concentration incubated with HFIP/PBS (20:80) solvent composites for 2 weeks prior to the measurements. This material is available free of charge via the Internet at <http://pubs.acs.org>.

## References and Notes

- (1) Ohnishi, S.; Takano, K. *Cell. Mol. Life Sci.* **2004**, *61*, 511–524.
- (2) Kaye, R.; Head, E.; Thompson, J. L.; McIntire, T. M.; Milton, S. C.; Cotman, C. W.; Glabe, C. G. *Science* **2003**, *300*, 486–489.
- (3) Lashuel, H. A.; Hartley, D. M.; Balakhaneh, D.; Aggarwal, A.; Teichberg, S.; Callaway, D. J. *J. Biol. Chem.* **2002**, *277*, 42881–42890.
- (4) Caughey, B.; Lansbury, P. T. *Annu. Rev. Neurosci.* **2003**, *26*, 267–298.
- (5) Kirkitadze, M. D.; Bitan, G.; Teplow, D. B. *J. Neurosci. Res.* **2002**, *69*, 567–577.

- (6) Bucciantini, M.; Giannoni, E.; Chiti, F.; Baroni, F.; Formigli, L.; Zurdo, J.; Taddei, N.; Ramponi, G.; Dobson, C. M.; Stefani, M. *Nature* **2002**, *416*, 507–511.
- (7) Demuro, A.; Mina, E.; Kayed, R.; Milton, S. C.; Parker, I.; Glabe, C. G. *J. Biol. Chem.* **2005**, *280*, 17294–17300.
- (8) Deshpande, A.; Mina, E.; Glabe, C.; Busciglio, J. *J. Neurosci.* **2006**, *26*, 6011–6018.
- (9) Masters, C. L.; Simms, G.; Weinman, N. A.; Multhaup, G.; McDonald, B. L.; Beyreuther, K. *Proc. Natl. Acad. Sci. U.S.A.* **1985**, *82*, 4245–4249.
- (10) Kang, J.; Lemaire, H. G.; Unterbeck, A.; Salbaum, J. M.; Masters, C. L.; Grzeschik, K. H.; Multhaup, G.; Beyreuther, K.; Muller-Hill, B. *Nature* **1987**, *325*, 733–736.
- (11) Olofsson, A.; Sauer-Eriksson, A. E.; Öhman, A. *J. Biol. Chem.* **2006**, *281*, 477–483.
- (12) Barrow, C. J.; Yasuda, A.; Kenny, P. T. M.; Zagorski, M. G. *J. Mol. Biol.* **1992**, *225*, 1075–1093.
- (13) Tomaselli, S.; Esposito, V.; Vangone, P.; van Nuland, N. A. J.; Bonvin, A. M. J. J.; Guerrini, R.; Tancredi, T.; Temussi, P. A.; Picone, D. *ChemBioChem* **2006**, *7*, 257–267.
- (14) Buck, M. *Q. Rev. Biophys.* **1998**, *31*, 297–355.
- (15) Crescenzi, O.; Tomaselli, S.; Guerrini, R.; Salvadori, S.; D'Ursi, A. M.; Temussi, P. A.; Picone, D. *Eur. J. Biochem.* **2002**, *269*, 5642–5648.
- (16) Halverson, K.; Fraser, P. E.; Kirschner, D. A.; Lansbury, P. T., Jr. *Biochemistry* **1990**, *29*, 2639–2644.
- (17) Lim, K. H.; Collver, H. H.; Le, Y.; Nagchowduri, P.; Kenney, J. M. *Biochem. Biophys. Res. Commun.* **2007**, *2*, 443–449.
- (18) Yang, D. S.; Yip, C. M.; Huang, T. H. J.; Chakrabartty, A.; Fraser, P. E. *J. Biol. Chem.* **1999**, *274*, 32970–32974.
- (19) Janek, K.; Rothmund, S.; Gast, K.; Beyermann, M.; Zipper, J.; Fabian, H.; Bienert, M.; Krause, E. *Biochemistry* **2001**, *40*, 5457–5463.
- (20) Walsh, D. M.; Hartley, D. M.; Kusumoto, Y.; Fezoui, Y.; Condrón, M. M.; Lomakin, A.; Benedek, G. B.; Selkoe, D. J.; Teplow, D. B. *J. Biol. Chem.* **1999**, *274*, 25945–25952.
- (21) Shao, H. Y.; Jao, S. C.; Ma, K.; Zagorski, M. G. *J. Mol. Biol.* **1999**, *285*, 755–773.
- (22) Zagorski, M. G.; Barrow, C. J. *Biochemistry* **1992**, *31*, 5621–5631.
- (23) Kirkitadze, M. D.; Condrón, M. M.; Teplow, D. B. *J. Mol. Biol.* **2001**, *312*, 1103–1119.
- (24) Serpell, L. C. *Biochim. Biophys. Acta* **2000**, *1502*, 16–30.
- (25) Soto, C.; Branes, M.; Alvarez, J.; Inestrosa, N. *J. Neurol. Chem.* **1994**, *63*, 1191–1198.
- (26) Kirschner, D.; Inouye, H.; Duffy, L.; Sinclair, A.; Lind, M.; Selkoe, D. *Proc. Natl. Acad. Sci. U.S.A.* **1987**, *84*, 6953–6957.
- (27) Barrow, C. J.; Zagorski, M. G. *Science* **1991**, *253*, 179–182.
- (28) Qahwash, I.; Weiland, K. L.; Lu, Y. F.; Sarver, R. W.; Kletzien, R. F.; Yan, R. Q. *J. Biol. Chem.* **2003**, *278*, 23187–23195.
- (29) Solomon, B. *DNA Cell Biol.* **2001**, *20*, 697–703.
- (30) Frenkel, D.; Katz, O.; Solomon, B. *Proc. Natl. Acad. Sci. U.S.A.* **2000**, *97*, 11455–11459.
- (31) Ormer, B. P.; Liu, L.; Murphy, R. M.; Kiessling, L. L. *J. Am. Chem. Soc.* **2006**, *128*, 11882–11889.
- (32) Soto, C.; Castaño, E. M.; Frangione, B.; Inestrosa, N. C. *J. Biol. Chem.* **1995**, *270*, 3063–3067.
- (33) Kirshenbaum, K.; Daggett, V. *Biochemistry* **1995**, *34*, 7629–7639.
- (34) Jarvet, J.; Damberg, P.; Bodell, K.; Eriksson, L. E. G.; Gräslund, A. *J. Am. Chem. Soc.* **2000**, *122*, 4261–4268.
- (35) LeVine, H., III. *Anal. Biochem.* **2004**, *335*, 81–90.
- (36) Wang, Y.; Goodson, T. *J. Phys. Chem. B* **2007**, *111*, 327–330.
- (37) Mukhopadhyay, S.; Nayak, P. K.; Udgaonkar, J. B.; Krishnamoorthy, G. *J. Mol. Biol.* **2006**, *358*, 935–942.
- (38) Maji, S. K.; Amsden, J. J.; Rothschild, K. J.; Condrón, M. M.; Teplow, D. B. *Biochemistry* **2005**, *44*, 13365–13376.
- (39) Pelet, S.; Previte, M. R.; So, P. T. C. *J. Biomed. Opt.* **2006**, *11*, 034017-1-11.
- (40) Cohen, B. E.; Pralle, A.; Yao, X.; Swaminath, G.; Gandhi, C. S.; Jan, Y. N.; Kobilka, B. K.; Isacoff, E. Y.; Jan, L. Y. *Proc. Natl. Acad. Sci. U.S.A.* **2005**, *102*, 965–970.
- (41) Jose, J.; Burgess, K. *Tetrahedron* **2006**, *62*, 11021–11037.
- (42) Tao, T. *FEBS Lett.* **1978**, *93*, 146–150.
- (43) Tleugabulova, D.; Czardybon, W.; Brennan, J. D. *J. Phys. Chem. B* **2004**, *108*, 10692–10699.
- (44) Paravastu, A. K.; Petkova, A. T.; Tycko, R. *Biophys. J.* **2006**, *90*, 4618–4629.
- (45) Kelly, J. W.; Balch, W. E. *Nat. Chem. Biol.* **2006**, *2*, 224–227.
- (46) Skoch, J.; Dunn, A.; Hyman, B. T.; Bacskai, B. J. *J. Biomed. Opt.* **2005**, *10*, 011007.
- (47) Bacskai, B. J.; Skoch, J.; Hickey, G. A.; Allen, R.; Hyman, B. T. *J. Biomed. Opt.* **2003**, *8*, 368–375.
- (48) Schafer-Hales, K. J.; Belfield, K. D.; Yao, S.; Frederiksen, P. K.; Hales, J. M.; Kolattukudy, P. E. *J. Biomed. Opt.* **2005**, *10*, 051402.
- (49) Andrade, M. A.; Chacón, P.; Merelo, J. J.; Morán, F. *Protein Eng.* **1993**, *6*, 383–390.
- (50) Merelo, J. J.; Andrade, M. A.; Prieto, A.; Morán, F. *Neurocomputing* **1994**, *6*, 443–454.
- (51) Greenfield, N.; Fasman, G. D. *Biochemistry* **1969**, *8*, 4108–4116.
- (52) Morrisett, J. D.; David, J. S. K.; Pownall, H. J.; Gotto, A. M. *Biochemistry* **1973**, *12*, 1290–1299.
- (53) Xu, C.; Webb, W. W. *J. Opt. Soc. Am. B* **1996**, *13*, 481–491.
- (54) Bhaskar, A.; Ramakrishna, G.; Lu, Z.; Twieg, R.; Hales, J. M.; Hagan, D. J.; Stryland, E. V.; Goodson, T., III. *J. Am. Chem. Soc.* **2006**, *128*, 11840–11849.
- (55) Vámosi, G.; Gohlke, C.; Clegg, R. M. *Biophys. J.* **1996**, *71*, 972–994.
- (56) Lahankar, S. A.; West, R.; Varnavski, O.; Xie, X.; Goodson, T., III; Sukhomlinova, L.; Twieg, R. *J. Chem. Phys.* **2004**, *120*, 337–344.
- (57) Ryderfors, L.; Mukhtar, E.; Johansson, L. B.-A. *Chem. Phys. Lett.* **2005**, *411*, 51–60.
- (58) Lührs, T.; Ritter, C.; Adrian, M.; Riek-Loher, D.; Bohrmann, B.; Döbeli, H.; Schubert, D.; Riek, R. *Proc. Natl. Acad. Sci. U.S.A.* **2005**, *102*, 17342–17347.
- (59) Torok, M.; Milton, S.; Kayed, R.; Wu, P.; McIntire, T.; Glabe, C. G.; Langen, R. *J. Biol. Chem.* **2002**, *277*, 40810–40815.
- (60) Huang, T. H.; Frazer, P. E.; Chakrabartty, A. *J. Mol. Biol.* **1997**, *269*, 214–224.
- (61) Huang, T. H.; Yang, D. S.; Plaskos, N. P.; Go, S.; Yip, C. M.; Frazer, P. E.; Chakrabartty, A. *J. Mol. Biol.* **2000**, *297*, 73–87.
- (62) Bateman, D. A.; Mclaurin, J.; Chakrabartty, A. *BMC Neurosci.* **2007**, *8*, 29.
- (63) Selwyn, J. E.; Steinfeld, J. I. *J. Phys. Chem.* **1972**, *76*, 762–774.
- (64) Marmé, N.; Knemeyer, J.-P.; Sauer, M.; Wolfrum, J. *Bioconjugate Chem.* **2003**, *14*, 1133–1139.
- (65) Packard, B. Z.; Topygin, D. D.; Komoriya, A.; Brand, L. *Proc. Natl. Acad. Sci. U.S.A.* **1996**, *93*, 11640–11645.
- (66) Makarov, N. S.; Drobizhev, M.; Rebane, A. *Opt. Express* **2008**, *16*, 4029–4047.
- (67) Varnavski, O.; Bäuerle, P.; Goodson, T., III. *Opt. Lett.* **2007**, *32*, 3083–3085.
- (68) Volkmer, A.; Hatrick, D. A.; Birch, D. J. S. *Meas. Sci. Technol.* **1997**, *8*, 1339–1349.
- (69) Lakowicz, J. *Principles of Fluorescence Spectroscopy*, 3rd ed.; Kluwer Academic/Plenum: New York, 2006.
- (70) Vogel, M.; Rettig, W.; Sens, R.; Drexhage, K. H. *Chem. Phys. Lett.* **1988**, *147*, 452–460.
- (71) Edman, L.; Mets, U.; Rigler, R. *Proc. Natl. Acad. Sci. U.S.A.* **1996**, *93*, 6710–6715.
- (72) Wennmalm, S.; Edman, L.; Rigler, R. *Proc. Natl. Acad. Sci. U.S.A.* **1997**, *94*, 10641–10646.
- (73) Eggeling, C.; Fries, J. R.; Brand, L.; Günther, R.; Seidel, C. A. M. *Proc. Natl. Acad. Sci. U.S.A.* **1998**, *95*, 1556–1561.
- (74) Doose, S.; Neuweiler, H.; Sauer, M. *ChemPhysChem* **2005**, *6*, 2277–2285.
- (75) Wang, L.; Gaigalas, A. K.; Blasic, J.; Holden, M. J. *Spectrochim. Acta, Part A* **2004**, *60*, 2741–2750.
- (76) Vaiana, A. C.; Neuweiler, H.; Schulz, A.; Wolfrum, J.; Sauer, M.; Smith, J. C. *J. Am. Chem. Soc.* **2003**, *125*, 14564–14572.
- (77) Kim, J.; Doose, S.; Neuweiler, H.; Sauer, M. *Nucleic Acids Res.* **2006**, *34*, 2516–2527.
- (78) Adams, D. M.; Brus, L.; Chidsey, C. E. D.; et al. *J. Phys. Chem. B* **2003**, *107*, 6668–6697.
- (79) Greenough, K. P.; Blanchard, G. J. *J. Phys. Chem. B* **2006**, *110*, 6351–6358.
- (80) Gryczynski, I.; Malak, H.; Lakowicz, J. R. *Chem. Phys. Lett.* **1995**, *245*, 30–35.
- (81) Fu, J.; Przhonska, O. V.; Padilha, L. A.; Hagan, D. J.; Van Stryland, E. W.; Belfield, K. D.; Bondar, M. V.; Slominsky, Y. L.; Kachkovski, A. D. *Chem. Phys.* **2006**, *321*, 257–268.
- (82) Unruh, J. R.; Gokulrangan, G.; Lushington, G. H.; Johnson, C. K.; Wilson, G. S. *Biophys. J.* **2005**, *88*, 3455–3465.
- (83) Brown, O.; Lopez, D.; Fuller, A. O.; Goodson, T., III. *Biophys. J.* **2007**, *93*, 1068–1078.